Short-range order quantification in transition metal fluoride glasses (TMFG) through EPR spectra simulation

1995 J. Phys.: Condens. Matter 7 4829

(http://iopscience.iop.org/0953-8984/7/25/008)

J. Phys.: Condens. Matter 7 (1995) 4829–4846. Printed in the UK

Short-range order quantification in transition metal fluoride glasses (TMFG) through EPR spectra simulation

C Legein†, J Y Buzaré‡, B Boulard† and C Jacoboni†

† Laboratoire des Fluorures, URA CNRS 449, Faculté des Sciences, Université du Maine, 72017 Le Mans Cédex, France

‡ Equipe de Physique de l'Etat Condensé, URA CNRS 807, Faculté des Sciences, Université du Maine, 72017 Le Mans Cédex, France

Received 18 November 1994

Abstract. Cr^{3+} and Fe^{3+} EPR spectra in transition metal fluoride glasses (TMFG), pyrochlore $CsZnGaF_6$ and amorphous GaF_3 are found to be very similar. Then, it is inferred that the constituent octahedra of all these disordered fluoride compounds are characterized by closely related distortions. Two short-range structural models, based on $CsZnGaF_6$ and GaF_3, are worked out with the aim of characterizing octahedra in TMFG. The $CsZnGaF_6$ model is developed using structural information on this compound. Amorphous GaF_3 structure is simulated by using molecular dynamics calculations starting from rhombohedral GaF_3. From the M–F distance and bonding angle distributions obtained from these two models, the Cr^{3+} and Fe^{3+} fine-structure parameter distributions are calculated with the help of the superposition model and finally the corresponding EPR spectra are computed. A good agreement is obtained simultaneously for the two local paramagnetic probes, which leads to a quantification of the short-range order in TMFG: constituent octahedra are only slightly distorted. It is interesting to note that the distributions of fine-structure parameters are very similar to the Czjzek ones previously used to simulate Cr^{3+} and Fe^{3+} spectra in TMFG.

1. Introduction

Most experimental data on degree of short-range ordering in disordered solids are traditionally obtained using diffraction techniques and EXAFS. They yield information on the number and radial distances of atoms in the first coordination shells but they give no information on their angular distribution. For instance, previous structural studies have shown that the transition metal fluoride glass (TMFG) network is built up of corner-sharing $M^{II}F_6$ and $M^{III}F_6$ octahedra [1, 2]. Other experimental techniques, able to investigate angular atomic distortions, are highly desirable.

One possibility is provided by ^{57}Fe Mössbauer spectroscopy. Several ferric amorphous fluorides have been investigated using Mössbauer spectroscopy ($NaFeF_4$, $KFeF_4$ and fluoride glasses [3], FeF_3, x HF [4–6] and FeF_3 obtained by vapour phase deposition [7]). The quadrupolar splitting distribution deduced from a point charge calculation on a random packing of corner-sharing octahedra network generated by computer was in good agreement with the Mössbauer results on amorphous FeF_3 [8]. These studies led to weakly distorted FeF_6 octahedra sharing corners in amorphous FeF_3 [7, 8].

Electron paramagnetic resonance (EPR) which is well known to provide valuable information about the local site symmetries provides another possibility to investigate angular atomic distortions. In order to make EPR an efficient tool for structural investigation

0953-8984/95/254829+18$19.50

of disordered materials, two problems have to be solved. The first one is the formalism used to explain the EPR spectra, the second one concerns the parametrization of the spectra in order to extract a description of the short-range ordering.

In a recent paper [9], we used the joint distribution $P(b_2^0, \lambda)$ of crystal-field parameters, where b_2^0 is the axial component and $\lambda = b_2^2/b_2^0$ is the asymmetry parameter ($0 \leqslant \lambda \leqslant 1$):

$$P(b_2^0, \lambda) = \frac{1}{(2\pi)^{1/2}\sigma^d}(b_2^0)^{d-1}\lambda\left(1 - \frac{\lambda^2}{9}\right)\exp - \frac{(b_2^0)^2(1 + \lambda^2/3)}{2\sigma^2} \qquad (1)$$

initially derived by Czjzek and co-workers [10] for a random packing of hard spheres and applied for the calculation of the electric field gradient in amorphous materials. It allows the accurate reconstruction of Cr^{3+} and Fe^{3+} spectra in TMFG (3d transition metal ions are well known to adopt a octahedral coordination in a fluoride medium, therefore they can be used as true local EPR probes). σ and d are two adjustable parameters; σ characterizes the interaction strength and d is the number of independent random variables. In TMFG, a simultaneous agreement for Cr^{3+} and Fe^{3+} ions at four different microwave frequencies (S, X, K and Q bands) was obtained with a single set of (σ, d) values. These sets of values are $\sigma = 2100 \times 10^{-4}$ cm^{-1} and $d = 3$ for Cr^{3+} and $\sigma = 810 \times 10^{-4}$ cm^{-1} and $d = 3$ for Fe^{3+} (figure 1). The $P(b_2^0, \lambda)$ function yields zero probability for $b_2^0 = 0$ and $\lambda = 0$. These results indicate a zero probability for the existence of high-symmetry octahedra, in agreement with the notion of disorder generally evoked in these glasses.

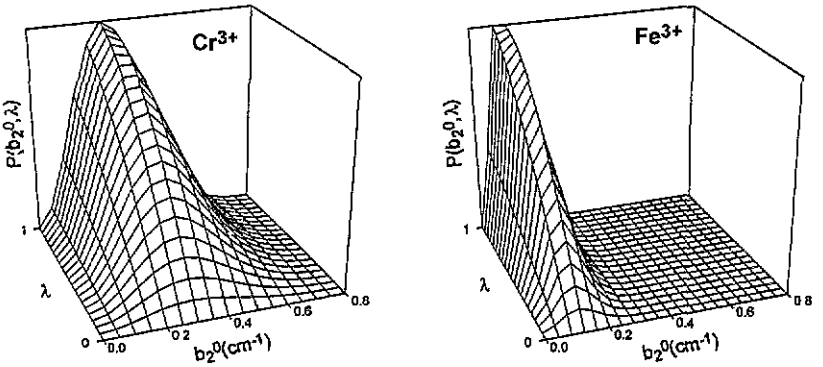

Figure 1. $P(b_2^0, \lambda)$ for Cr^{3+} ($\sigma = 0.21$ cm^{-1} and $d = 3$) and Fe^{3+} ($\sigma = 0.081$ cm^{-1} and $d = 3$).

The present paper deals with an attempt to solve the second problem.

The superposition model introduced by Newman [11] is presented in section 3. It allows the estimation of fine-structure parameters knowing the local structure. As the opposite operation is impossible, the elaboration of structural models (atomic coordinate distribution) is essential in order to extract a quantitative description of short-range ordering (*distance and bonding angle distributions*). *In this paper, two short-range structural models* are presented with the aim of characterizing octahedral distortions in TMFG. They are worked out from two disordered fluoride compounds built up of MF_6 octahedra in which Cr^{3+} and Fe^{3+}, used as local probes, give EPR spectra similar to those obtained in TMFG.

(i) The first one, presented in section 4, is based on $CsZnGaF_6$ which has a cubic pyrochlore $RbNiCrF_6$-type structure characterized by a statistical distribution of octahedrally coordinated 3d ions on the same site (16c, SG: $Fd3m$) leading to a disorder related to slight displacements of anions as shown by EXAFS [12].

(ii) In section 5, the second one, amorphous GaF_3, is presented; the structure of this disordered compound is modelled by the use of molecular dynamics (MD) calculations on rhombohedral GaF_3.

2. Experimental procedures

EPR spectra were studied on TMFG derived from two basic glasses, PZG (35 PbF_2, 24 ZnF_2, 34 GaF_3, 5 YF_3, 2 AlF_3 mol%) [13] and PBI (19 PbF_2, 23 BaF_2, 47 InF_3, 2 AlF_3, 4.5 YF_3, 4.5 SrF_2 mol%) [14], on crystalline $CsZnGaF_6$ and on amorphous GaF_3.

Owing the fact that fluoride compounds are moisture sensitive, all preparative work was done inside a dry glove-box.

(i) In glasses, CrF_3 and FeF_3 were added at low concentration (0.20 or 0.25 wt%). After preliminary mixing, the melt was placed in a covered platinum crucible, heated at 800 °C and then cast into a preheated (200 °C) mould.

(ii) Crystalline $CsZnGaF_6$ was obtained from solid state reaction of ($CsF + ZnF_2 + GaF_3 + CrF_3$ or FeF_3) mixture, in a sealed platinum tube at 650 °C. $CsZnFeF_6$ used for Mössbauer study was also obtained by solid state reaction at 630 °C.

(iii) Amorphous GaF_3:Fe^{3+} was obtained by vapour phase deposition [15]. The evaporations were conducted in a 6 cm diameter Pyrex vessel connected to a vacuum system allowing pressure around 10^{-4} mbar in the vessel. The platinum crucible containing the premelted starting charge ($GaF_3 + FeF_3$) was heated with an RF coil. Amorphous GaF_3:Cr^{3+} was very difficult to synthesize because GaF_3 has a higher vapour pressure than CrF_3. The chemical composition of deposited phases was analysed by ICP (Perkin Elmer 6500).

The EPR X band (9.5 GHz) and S band (4 GHz) spectra were recorded on a Bruker spectrometer; measurements at variable temperature (X band) were achieved by using an Oxford Cryostat. Q band spectra were recorded by P Simon in the CRPHT (UP CNRS 4212).

The $CsZnFeF_6$ Mössbauer spectrum was recorded and analysed by J M Grenèche (Equipe de Physique de l'Etat Condensé, URA CNRS 807).

3. The superposition model

The Cr^{3+} ($3d^3$, $S = 3/2$) and Fe^{3+} ($3d^5$, $S = 5/2$) spin Hamiltonian fine-structure term is

$$H_{sf} = \sum_{n=0}^{2S} \sum_{m=-n}^{n} B_n^m O_n^m \qquad \text{with } n \text{ an even number.} \tag{2}$$

By neglecting higher-order terms for Fe^{3+}, it becomes

$$H_{sf} = \tfrac{1}{3}(b_2^0 O_2^0 + b_2^2 O_2^2 + b_2^{-2} O_2^{-2} + b_2^1 O_2^1 + b_2^{-1} O_2^{-1}). \tag{3}$$

The O_n^m expressions are given in table 1.

The superposition model [11] assumes that the spin Hamiltonian parameters depend on the local surrounding of the paramagnetic ion through the law

$$b_n^m = \sum_i b_n(R_i) K_n^m(\theta_i, \varphi_i) \tag{4}$$

where i runs over the nearest neighbours at coordinates R_i, θ_i and φ_i. The $K_n^m(\theta_i, \varphi_i)$ terms are given in table 1 for $n = 2$.

Table 1. O_n^m and K_n^m expressions.

O_n^m	K_n^m
$O_2^0 = 3S_z^2 - S(S+1)$	$K_2^0 = \frac{1}{2}(3\cos^2\theta - 1)$
$O_2^1 = \frac{1}{2}(S_zS_x + S_xS_z)$	$K_2^1 = 3\sin 2\theta\cos\varphi$
$O_2^{-1} = \frac{1}{2}(S_zS_y + S_yS_z)$	$K_2^{-1} = 3\sin 2\theta\sin\varphi$
$O_2^2 = S_x^2 - S_y^2$	$K_2^2 = \frac{3}{2}\sin^2\theta\cos 2\varphi$
$O_2^{-2} = S_xS_y + S_yS_x$	$K_2^{-2} = \frac{3}{2}\sin^2\theta\sin 2\varphi$

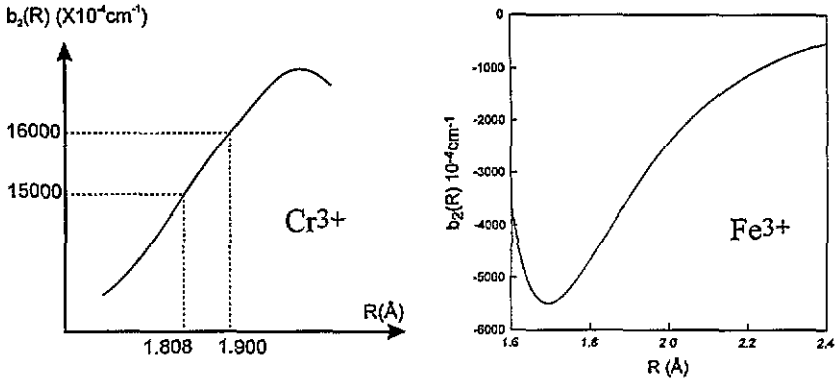

Figure 2. $b_2(R)$ for Cr^{3+} and Fe^{3+} in fluoroaluminates from [16].

The radial functions $b_n(R_i)$ depend on the probe and ligand type. From several experimental results on fluoroaluminate single crystals, Houlbert was able to determine $b_2(R)$ for Cr^{3+} and Fe^{3+}: for Fe^{3+} a Lennard-Jones-type law

$$b_2(R) = -A\left(\frac{R_0}{R}\right)^n + B\left(\frac{R_0}{R}\right)^m \tag{5}$$

was fitted with $A = 2.4\ \text{cm}^{-1}$, $B = 1.85\ \text{cm}^{-1}$, $R_0 = 1.693$ Å, $n = 10$ and $m = 13$ and for Cr^{3+} only the curve trend was given [16] (figure 2). If we compare the relative $b_2(R)$ variations for the two paramagnetic probes, for $R = 1.9$ Å it is found that

$$\Delta b_2(R)/[b_2(R)\,\Delta R] = 0.68\ \text{Å}^{-1}$$

for Cr^{3+} and

$$\Delta b_2(R)/[b_2(R)\,\Delta R] = 3.37\ \text{Å}^{-1}$$

for Fe^{3+}.

Thus, Cr^{3+} is less sensitive to radial distortions and consequently more sensitive to angular distortions than Fe^{3+}. Therefore, it may be interesting to work with both of these paramagnetic probes to ascertain our structural investigations.

The application of the superposition model with these $b_2(R)$ functions for Cr^{3+}- and Fe^{3+}-doped AlF_3, GaF_3 and InF_3, presented in [17], gives the best agreement between experimental and calculated b_2^0 values for GaF_3. This result may be related to a small lattice relaxation around the probes resulting from the closeness of ionic radii of Ga^{3+} and Cr^{3+} or Fe^{3+}. On the other hand, the agreement between calculated and experimental

parameters is less satisfying for AlF_3 and InF_3. Then, it is more advisable for extracting a quantitative description of short-range ordering to have close radii for probe and host ions. Cr^{3+} and Fe^{3+} are therefore well adapted for $CsZnGaF_6$, amorphous GaF_3 and PZG glass EPR studies.

4. $CsZnGaF_6$

4.1. Introduction

In the $A^IM^{II}M^{III}F_6$ pyrochlore structure (spatial group $Fd3m$), a statistical distribution of the M^{II} and M^{III} cations is imposed on the 16c site; the network is built up of corner sharing MF_6 octahedra (figure 3). At room temperature, diffraction studies have led to a mean value of the M–F distance $d_{M-F} = 1.92$ Å for $CsZnGaF_6$ with an abnormally high thermal agitation for F^- anions. The true M^{II}–F and M^{III}–F distances have been determined by EXAFS [12]: they are respectively equal to 2.01 Å and 1.89 Å as expected from the ionic radii sum (2.025 Å and 1.905 Å [13]). The two different values for Zn–F and Ga–F distances correspond to a small spreading of the M–M distances in agreement with diffraction results (standard thermal agitation) but they imply a very important variation in the M–F–M angle (Zn–F–Zn = 129.5%, Zn–F–Ga = 137.8% and Ga–F–Ga = 149.1%) (figure 4).

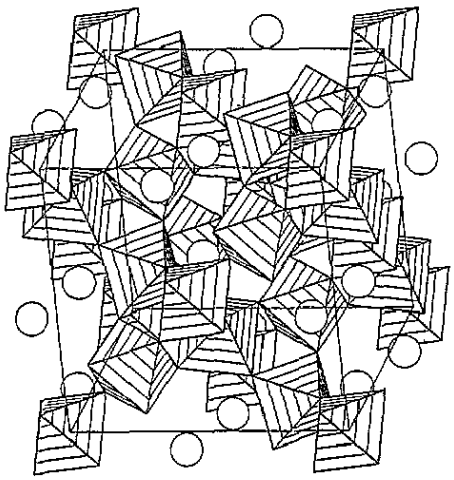

Figure 3. $CsZnGaF_6$ structure.

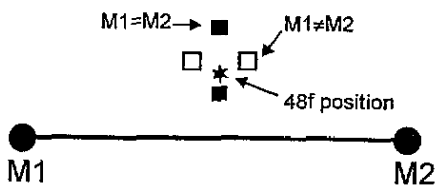

Figure 4. Position of F^- ions between M1, M2 cations in pyrochlore $AM^{II}M^{III}F_6$ from [12].

The $CsZnGaF_6$:Fe^{3+} spectrum simulation has been briefly presented in a previous paper [19]. The validity of this model for both Fe^{3+} and Cr^{3+} spectra in TMFG is discussed in this paper.

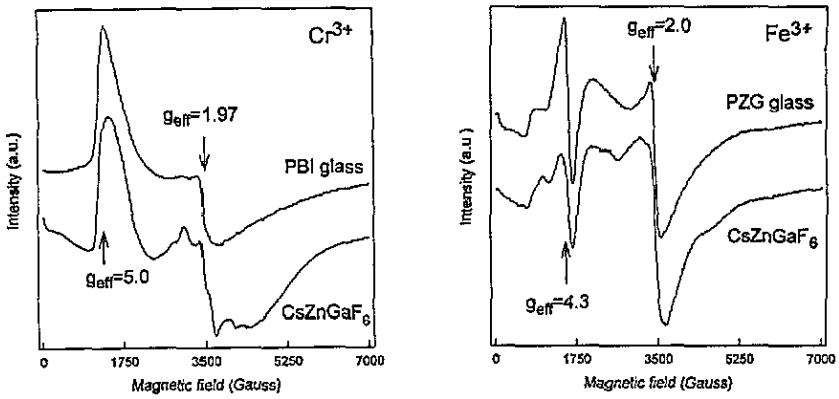

Figure 5. Cr^{3+} X band EPR spectra in PBI glass (1.50 wt% CrF_3; $T = 4$ K; $\nu = 9.43$ GHz) and $CsZnGaF_6$ (1.00 wt% CrF_3; $T = 4$ K; $\nu = 9.50$ GHz); Fe^{3+} X band EPR spectra in PZG glass (0.25 wt% FeF_3; $T = 4$ K; $\nu = 9.49$ GHz) and $CsZnGaF_6$ (1.00 wt% FeF_3; $T = 4$ K; $\nu = 9.50$ GHz)

4.2. EPR investigations

$CsZnGaF_6$:Cr^{3+} and Fe^{3+} EPR spectra are nearly similar to Cr^{3+} and Fe^{3+} spectra in TMFG (figure 5).

(i) In these compounds Fe^{3+} spectra exhibit two main resonances at $g_{eff} = 4.3$ and $g_{eff} = 2.0$. The ratio of intensities $I_{g_{eff}=2}/I_{g_{eff}=4.3}$ is slightly higher for $CsZnGaF_6$ than in TMFG at equal concentration.

(ii) Cr^{3+} EPR spectra exhibit two main resonances at $g_{eff} = 5.0$ and $g_{eff} \approx 2.0$. As for Fe^{3+}, the ratio $I_{g_{eff}\approx 2}/I_{g_{eff}=5.0}$ is higher for $CsZnGaF_6$ than in TMFG.

The constituent octahedra of TMFG and $CsZnGaF_6$ may be therefore assumed to be characterized by nearly the same distortions in the two networks; the intensity ratio values give evidence that the constituent octahedra in TMFG are slightly more distorted than the octahedra in $CsZnGaF_6$.

As in the previous study devoted to TMFG [9], we have recorded Cr^{3+} and Fe^{3+} spectra in $CsZnGaF_6$ at S and Q bands in order to confirm that the fine-structure parameters are nearly the same in TMFG and $CsZnGaF_6$.

(i) For Cr^{3+}, the microwave frequency increase leads to an increase of the $g_{eff} = 1.97$ line intensity at the expense of the $g_{eff} = 5.0$ one. The S band ($\nu = 4$ GHz) spectrum is composed of a single resonance at $g_{eff} = 5.0$. The Q band ($\nu = 35$ GHz) spectrum presents a very weak resonance at $g_{eff} = 5.0$ (weaker than the TMFG one).

(ii) For Fe^{3+}, a similar behaviour is observed. At S band the $g_{eff} = 4.3$ resonance predominates. The Q band spectrum is constituted of a single resonance at $g_{eff} = 2.0$.

The Cr^{3+} and Fe^{3+} S and Q band spectra are nearly the same in TMFG and $CsZnGaF_6$. Thus, as for TMFG, a single crystal-field parameter distribution may be used to account for Cr^{3+} and Fe^{3+} spectra in $CsZnGaF_6$. σ and d values characterizing Cr^{3+} and Fe^{3+} spectra in $CsZnGaF_6$ are found to be very close to those in TMFG. d being an integer, a variation of d value should lead to an important variation of σ. Assuming $d = 3$ for $CsZnGaF_6$ as in TMFG the σ values are slightly smaller than the corresponding values in TMFG: 0.21 cm^{-1} for Cr^{3+} and 0.081 cm^{-1} for Fe^{3+}.

4.3. Mössbauer investigation on $CsZnFeF_6$

The $A^IM^{II}M^{III}F_6$ pyrochlore structure type has been previously studied by Mössbauer spectroscopy; the existence of two different iron sites has been shown in $CsFe^{II}CrF_6$ and $CsFe^{II}VF_6$ [20] and in $CsNiFe^{III}F_6$ [21]. Those results are inconsistent with our single-crystal-field distribution assumption for $CsZnGaF_6$. Thus, we decided to perform Mössbauer spectroscopy on $CsZnFeF_6$, which is an Fe^{III} pyrochlore. The disorder might be similar in $CsZnGaF_6$ and $CsZnFeF_6$ since Ga^{3+} and Fe^{3+} ionic radii are very close (0.620 Å and 0.645 Å respectively [18]).

Table 2. *d* values for some amorphous fluoride compounds.

Compound	*d*	Reference
Deposited amorphous FeF_3	2	[4]
Amorphous FeF_3, *x* HF	2.7	[4]
Amorphous $AFeF_4$ (A = Na, K)	2	[3]
PMF glass (PbF_2–MnF_2–FeF_3)	2	[3]
$CsZnFeF_6$	2.9	This work

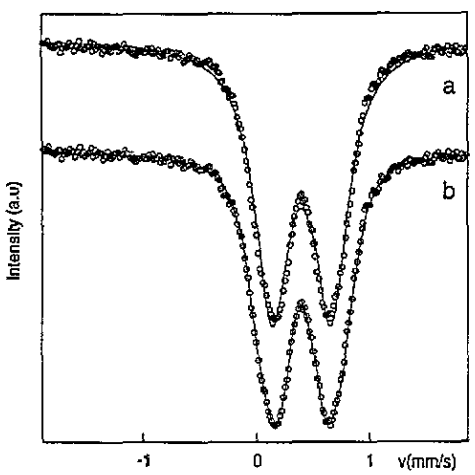

Figure 6. Mössbauer spectrum (dots) at 77 K of $CsZnFeF_6$ with (a) one-quadrupolar-component fit or (b) $P(\Delta)$ fit.

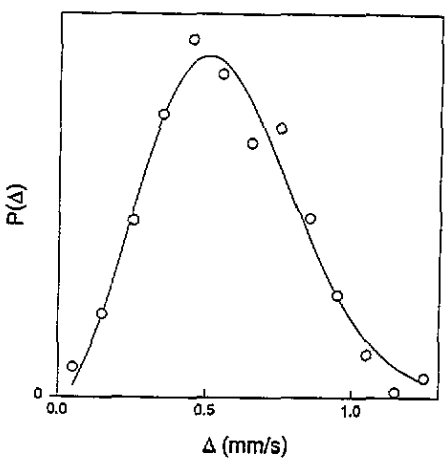

Figure 7. Quadrupolar splitting distribution $P(\Delta)$ for $CsZnFeF_6$ (dots: from $CsZnFeF_6$ Mössbauer spectrum fit, continuous line: analytical form of $P(\Delta)$).

The reconstruction of the experimental spectrum involves two fitting procedures. First, the adjustment with a Lorentzian line doublet leads to the hyperfine parameter values (isomer shift IS and quadrupole splitting Δ): $IS = 0.45$ mm s^{-1} and $\Delta = 0.55$ mm s^{-1} which are characteristic of Fe^{3+} ions in octahedral coordination. Secondly, because of the disagreement between the calculated and the experimental spectra we introduce a discrete distribution of quadrupole splitting $P(\Delta)$, the isomer shift being constant (figure 6). The shape of $P(\Delta)$ is consistent with the following expression:

$$P(\Delta) = \frac{\Delta^{d-1}}{\sigma^d} \exp\left(-\frac{\Delta^2}{2\sigma^2}\right) \tag{6}$$

with $\Delta = V_{ZZ}\sqrt{1+\eta^2/3}$ and $\eta = (V_{XX} - V_{YY})/V_{ZZ}$ derived by Czjzek from the joint distribution $P(V_{ZZ}, \eta)$ established in the case of a random packing of hard spheres for a nuclear spin $I = \frac{3}{2}$ [22]. The ratio $q = \langle\Delta^2\rangle/\langle\Delta\rangle^2$ can be used to characterize the number of independent random components of the electric field gradient (EFG), d [3]. At 300 K and 77 K, for $CsZnFeF_6$, the q value is 1.17 leading to d close to three. The $P(\Delta)$ distribution function refinement (figure 7) yields a d value equal to 2.9. The d parameter values deduced from the quadrupole splitting distribution for amorphous fluoride compounds are compared in table 2. They are always found to be between two and three.

It may be outlined that the Mössbauer spectra simulation leads to a quadrupolar-field-splitting distribution $P(\Delta)$ whereas EPR allows us to reach the $P(b_2^0, \lambda)$ distribution through the dependence of energy levels on the magnetic field. Nevertheless, the $P(\eta)$ associated with the quadrupolar splitting distribution deduced from a point charge calculation on a random packing of corner-sharing octahedra structure [8] yields zero probability for $\eta = 0$ [23] consistent with the distribution used for EPR spectra simulation. The EPR and Mössbauer studies lead to the existence of a single distribution of crystal-field parameters or quadrupole splitting in $CsZnGaF_6$ or $CsZnFeF_6$. These distributions $P(b_2^0, \lambda)$ and $P(\Delta)$ are characterized by the same d value.

4.4. Modelling approach of TMFG based on $CsZnGaF_6$

The construction of the model taking into account the previous structural results and its comparison to the experimental results are achieved in a four-step procedure.

Step I. The Zn^{2+} and Ga^{3+} cations are randomly distributed on the 16c site: each MF_6 octahedron is surrounded by six cations. The theoretical configuration probabilities $(1/2^6)C_6^n$ are

$6M^{II}$	1/64	$5M^{II}, M^{III}$	6/64	$4M^{II}, 2M^{III}$	15/64
$3M^{II}, 3M^{III}$	20/64	$2M^{II}, 4M^{III}$	15/64	$1M^{II}, 5M^{III}$	6/64.
		$6M^{III}$	1/64		

It is necessary to extend the primitive unit cell by 4^3 ($Z = 512$) in order to obtain probabilities in agreement with the theoretical values.

Step II. The F^- atomic positions (x, y, z) are calculated assuming that

(i) the cations are fixed;

(ii) the F^- anions stay in the M–F–M plane of the $CsZnGaF_6$ ideal structure;

(iii) the distance distributions of M^{II}–F and M^{III}–F are Gaussian (probability proportional to $\exp-[(d-d_0)^2/2(\Delta d)^2]$) and centred around values determined by EXAFS. Δd is an adjustable parameter. One distance is randomly attributed to each M–F bond.

Step III. From the atomic positions of Ga^{3+} and F^- ions, the 512 sets of fine-structure parameters $(b_2^0, b_2^1, b_2^{-1}, b_2^2, b_2^{-2})$ are computed with the help of the superposition model presented in section 3.

Step IV. The sets of fine-structure parameters are expressed in their eigenframe leading to b_2^0 and b_2^2 values directly comparable to those used in Czjzek's distribution.

The line shape calculation procedure was presented in [9]; here we have used a discrete $P(b_2^0, \lambda)$ distribution whereas, in [9], $P(b_2^0, \lambda)$ had an analytical form.

(i) Several sets of d_0 and Δd values can give a good agreement between observed and calculated spectra for $CsZnGaF_6$:Fe^{3+}. Among these values, we have retained d_0(Ga–F) = 1.91 Å, d_0(Zn–F) = 1.99 Å and Δd = 0.025 Å for which a good agreement is obtained

simultaneously for $CsZnGaF_6$:Fe^{3+} and $CsZnGaF_6$:Cr^{3+} [19]. For Cr^{3+}, a satisfactory agreement is difficult to reach with M–F distance values determined by EXAFS. This result, related to the high sensitivity of Cr^{3+} to angular distortions, points out that the bonding angle distribution obtained in this case has too large values due to the very large difference between Zn–F and Ga–F distances.

(ii) For TMFG a good agreement is obtained simultaneously for Cr^{3+} and Fe^{3+} with d_0(Ga–F) = 1.91 Å, d_0(Zn–F) = 1.99 Å and Δd = 0.03 Å (figure 8). Constitutive GaF_6 octahedra are therefore slightly more distorted in TMFG than in $CsZnGaF_6$.

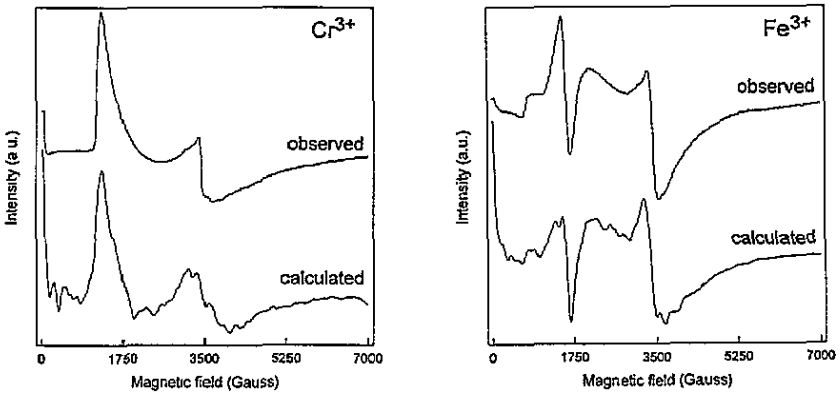

Figure 8. Observed and calculated Cr^{3+} and Fe^{3+} X band EPR spectra in TMFG (Cr^{3+}: PBI glass, 0.20 wt% CrF_3, T = 4 K, ν = 9.42 GHz; Fe^{3+}: PZG glass, 0.25 wt% FeF_3, T = 4 K, ν = 9.49 GHz).

The parameters used for the calculated spectra are:

Cr^{3+}	$g = 1.98$	$L_0 = 60$ G	$n\theta = 39$	$n\varphi = 39$
Fe^{3+}	$g = 2.002$	$L_0 = 60$ G	$n\theta = 27$	$n\varphi = 27$.

L_0 is the isotropic line width and $n\theta$ and $n\varphi$ the number of poles on θ and φ [3].

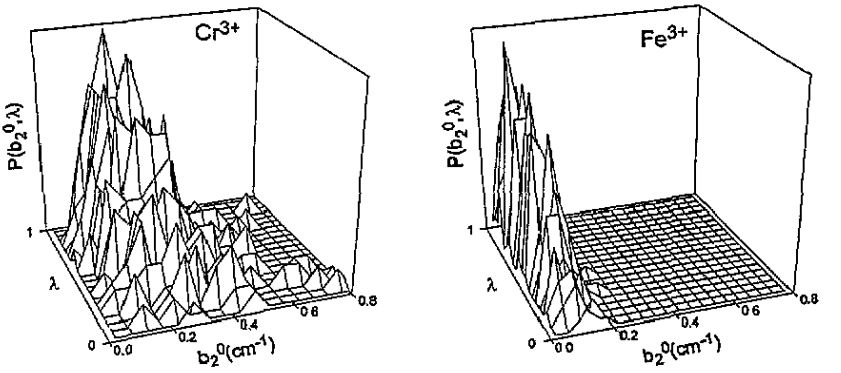

Figure 9. Fine-structure parameters (b_2^0, λ) for Cr^{3+} and Fe^{3+} in TMFG.

The background noise of the calculated spectra is higher than for reconstruction using analytical function [9] because the number of fine-structure parameter sets (b_2^0, λ) is smaller (512 instead of 49^2 for Cr^{3+} or 33^2 for Fe^{3+}).

4.5. Discussion

The corresponding fine-structure parameter distributions are shown in figure 9. They are nearly the same as the corresponding Czjzek distributions; they reduce to zero for b_2^0 and λ equal to zero; the higher probability values are observed for the same values ($\lambda = 1 - b_2^0 = 0.1$ cm^{-1} for Fe^{3+} and $\lambda = 1 - b_2^0 = 0.25$ cm^{-1} for Cr^{3+}). Therefore the use of the Czjzek distribution for Cr^{3+} and Fe^{3+} spectra reconstruction in TMFG is—*a posteriori*—validated.

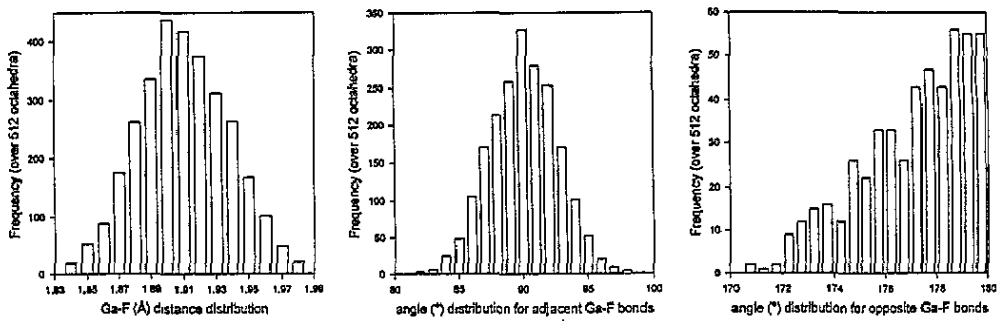

Figure 10. Ga–F distance, angle for adjacent Ga–F bonds and angle for opposite Ga–F bonds distributions.

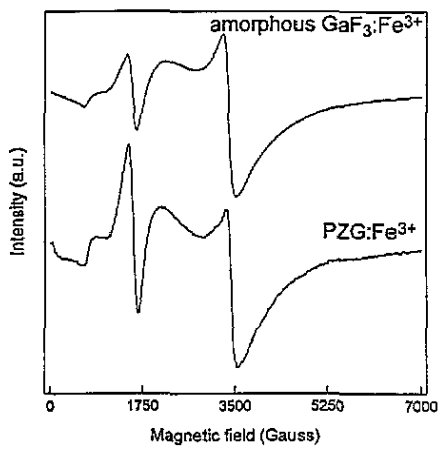

Figure 11. Fe^{3+} X band EPR spectra in PZG glass (0.25 wt% FeF_3; $T = 4$ K; $\nu = 9.49$ GHz) and amorphous GaF_3 (2.50 wt% FeF_3; $T = 4$ K; $\nu = 9.43$ GHz).

In order to characterize the $M^{III}F_6$ octahedra disorder, we have represented the $M^{III}F$ distance distribution, the angle distribution between one Ga–F bond and the four nearly perpendicular Ga–F bonds and finally the angle distribution between opposite Ga–F bonds (figure 10). Our model leads to slightly distorted $M^{III}F_6$ octahedra; the distance and angle distributions are relatively narrow: the $M^{III}F_6$ distances are nearly all in the $d_0 \pm 0.04$ Å range, the angular distortions from the regular octahedron are less than 5°.

5. Molecular dynamics on GaF_3

5.1. Introduction

Like the TMFG:Fe^{3+} spectra, the amorphous GaF_3:Fe^{3+} EPR spectrum exhibits two main resonances at $g_{eff} = 4.3$ and $g_{eff} = 2.0$ (figure 11). The ratio of intensities $I_{g_{eff}=2}/I_{g_{eff}=4.3}$ is higher for GaF_3 because the FeF_3 concentration is higher for GaF_3. At equal temperature and concentration these ratios would be very close. In TMFG and amorphous GaF_3, the distortions of the constituent GaF_6 octahedra are therefore similar. So, it was interesting to simulate the amorphous GaF_3 structure using molecular dynamics (MD) in order to reconstruct EPR spectra and then determine octahedron distortions in amorphous GaF_3 and in TMFG. A previous MD study on GaF_3 with random atomic position generation [24] has led to strongly distorted octahedra in contradiction with the narrower Ga–F distance distribution deduced from EXAFS [25]. The use of the MD method, starting from atomic positions of a crystalline compound, allows to prevent important distortions of the octahedra; it consists of relaxing the structure so far as the potential permits it.

5.2. MD principle

5.2.1. Potential expression. The simulation was performed using a modified Born–Mayer pair potential [26]:

$$V_{ij}(r) = bA_{ij}\exp\left(\frac{\sigma_i + \sigma_j - r}{\rho}\right) + \frac{Z_i Z_j e^2}{r} \tag{7}$$

where b is a repulsive constant which is the same for all fluoride compound ($b = 0.19 \times 10^{-12}$ erg) [27]. σ is the ionic radius and Z the ionic charge. According to Busing [28], the softness factor ρ is the same for all pairs (0.29 Å) and $A_{ij} = 1 + Z_i/n_i + Z_j/n_j$ with n the number of valence electrons. σ(Ga) has been refined in order that Ga–F distances remain equal to 1.89 Å on the average (table 3).

Table 3. MD parameters used for pair potential.

Parameters	Ga–Ga	Ga–F	F–F
B_{ij}^{a}	5107	2065	726
$\sigma_i + \sigma_j$ (Å)	2.82	2.647	2.474 [22]

[a] $B_{ij} = bA_{ij}\exp[(\sigma_i + \sigma_j)/\rho] \times 10^{12}$erg.

In order to reduce the calculation time, the pair Coulomb potentials are usually approximated and Coulomb forces truncated:

$$V_{ij}(r) = \left[bA_{ij}\exp\left(\frac{\sigma_i + \sigma_j - r}{\rho}\right) + \frac{Z_i Z_j e^2}{r}\right]\left[1 - \left(\frac{r}{R_{max}}\right)^6\right] \tag{8}$$

with $R_{max} = 9$ Å.

5.2.2. Calculation procedure. The initial set of atomic positions corresponds to rhombohedral GaF_3 [29]. The network is built up of corner-sharing GaF_6 octahedra (figure 12). The original size of the box is $4a$, $4b$ and $2c$ (768 atoms; $Z = 192$). A random Maxwellian distribution is used to determine the initial velocity of each atoms.

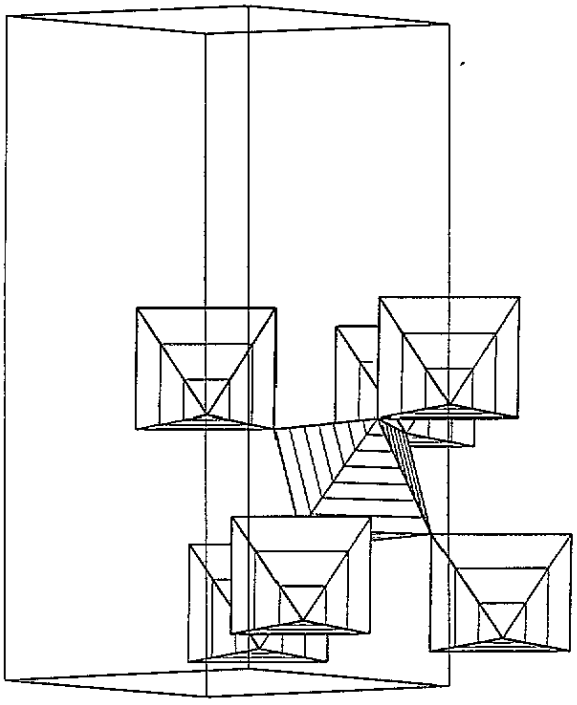

Figure 12. GaF_3 structure, hexagonal cell: $a = 5.002$ Å, $c = 12.973$ Å.

After the force on each atom is computed, the atomic positions and velocities are updated every time step δt ($\delta t = 2 \times 10^{-15}$ s). The atomic positions are calculated with the simple algorithm suggested by Verlet [30]. At each time step, the atom velocities are increased or decreased in order to scale kinetic energy ($E_k = \frac{1}{2}\sum_i M_i v_i^2$) compared with total energy ($E = \sum \frac{3}{2}kT$).

The calculation is done in two steps:

(i) structure relaxation; this step lasts 100 to $300\delta t$ according to the temperature so atoms can cover approximately the same distance (≈0.04 Å);

(ii) atomic position accumulation every $100\delta t$ in order to obtain 576 different configurations for GaF_6 octahedra. Thus, the number of fine-structure parameter sets is close to the one used within the preceding model.

5.3. Results

The calculations were performed for several values of the temperature (proportional to total energy) between 25 and 300 K. The results of the MD relaxation of GaF_3 for 25 K, 75 K, 120 K and 200 K are shown in figure 13, 14 and 15.

Figure 13 displays the changes in Ga–F distance distribution, angle between Ga–F perpendicular bonds distribution and angle between opposite Ga–F bonds distribution. The distribution width increases with temperature, GaF_6 octahedra become obviously more and more distorted. Whatever the temperature value, the Ga–F distance distribution remains centred at 1.89 Å which is the Ga–F distance in rhombohedral GaF_3 and the angle between

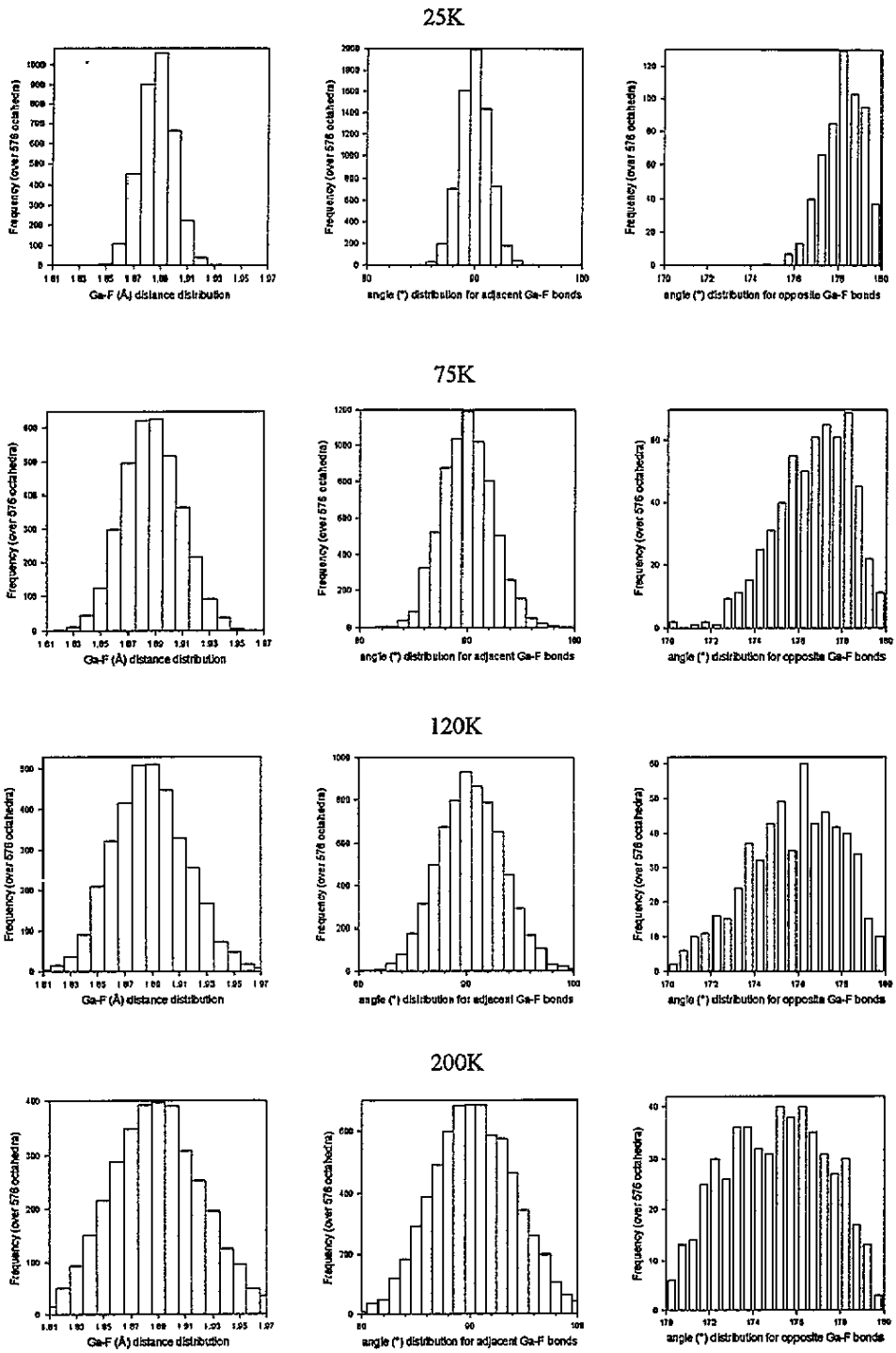

Figure 13. Ga–F distance, angle for adjacent Ga–F bonds and angle for opposite Ga–F bonds distributions at different temperatures.

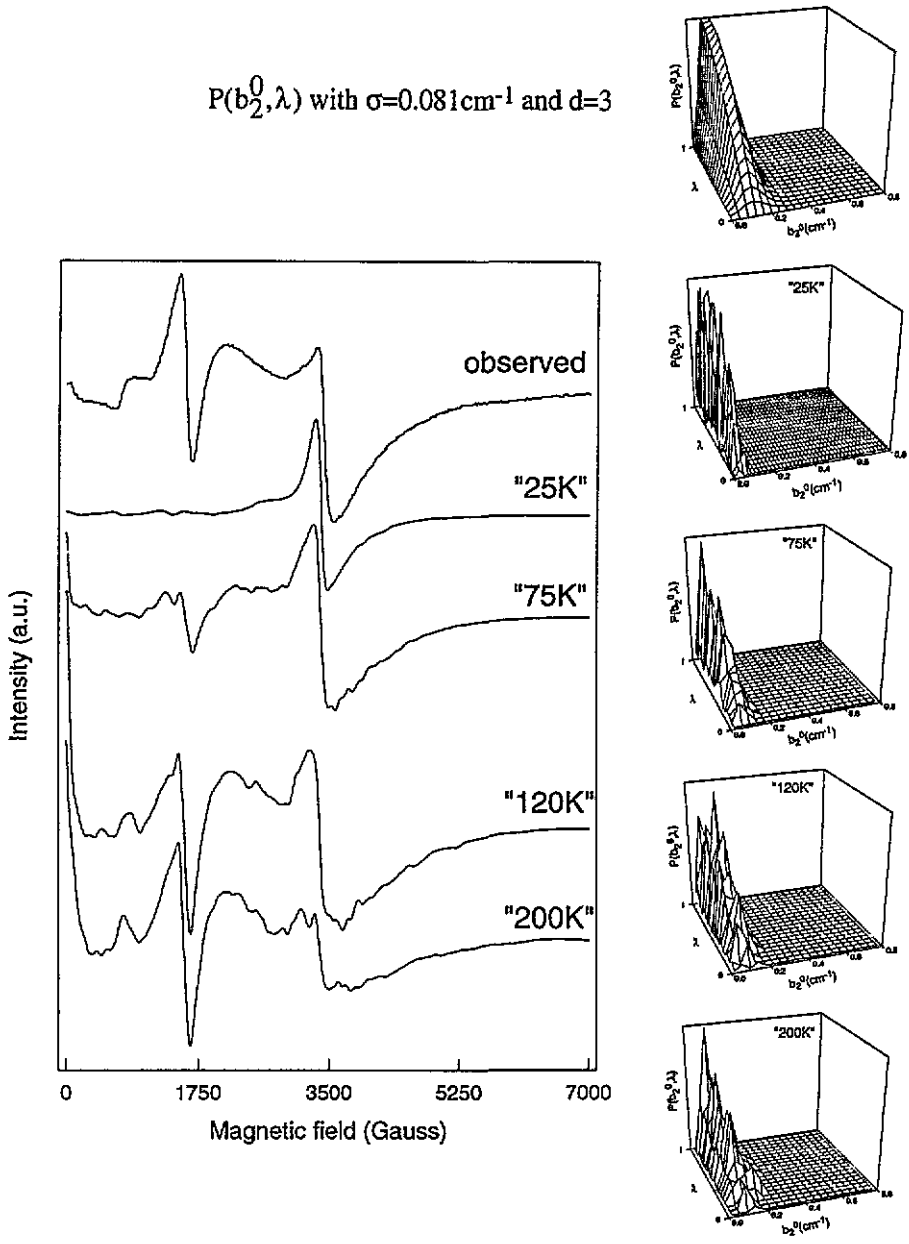

Figure 14. Observed (PZG glass, 0.25 wt% FeF_3, $T = 4$ K, $\nu = 9.49$ GHz) and calculated X band EPR spectra and fine structure parameters (b_2^0, λ) for Fe^{3+} in TMFG; the Czjzek distribution used for Fe^{3+} simulation is shown at the top of the figure.

perpendicular bonds distribution remains centred at 90°. The maximum of the distribution of the angles between opposite bonds moves out from 180° when temperature increases.

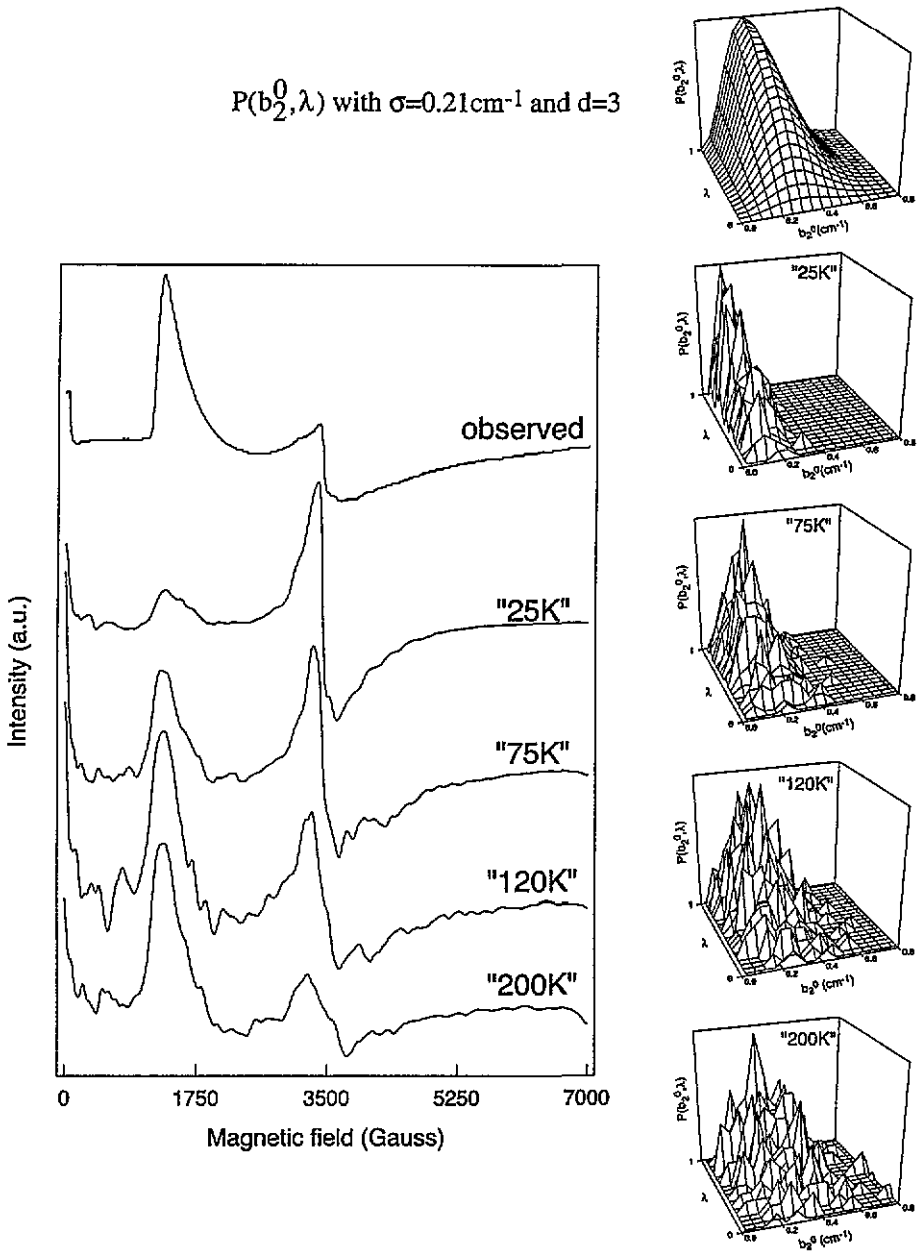

Figure 15. Observed (PBI glass, 0.20 wt% CrF_3, $T = 4$ K, $\nu = 9.42$ GHz) and calculated X band EPR spectra and fine-structure parameters (b_2^0, λ) for Cr^{3+} in TMFG; the Czjzek distribution used for Cr^{3+} simulation is shown at the top of the figure.

This behaviour was not observed in the $CsZnGaF_6$ model (figure 10), where this maximum remains at 180°, this is related to the assumption of fixed cations and F^- ions in the ideal

M–F–M plan.

Figures 14 and 15 show the corresponding Cr^{3+} and Fe^{3+} calculated spectra and fine structure parameter distributions. The parameters used for the calculated spectra are

Cr^{3+}	$g = 1.97$	$L_0 = 60$ G	$n\theta = 49$	$n\varphi = 49$
Fe^{3+}	$g = 2.002$	$L_0 = 60$ G	$n\theta = 27$	$n\varphi = 27$

(except for Fe^{3+} at $T = 120$ K: $n\theta = 25$, $n\varphi = 25$). When the temperature increases, the low-field resonance intensity increases for Cr^{3+} ($g_{eff} = 5.0$) and Fe^{3+} ($g_{eff} = 4.3$). Whatever the temperature value, the fine structure parameter distribution reduces to zero for b_2^0 and λ equal to zero and the highest values of $P(b_2^0, \lambda)$ are observed for $\lambda = 1$. Therefore, these distributions have the same properties as the Czjzek ones. The fine structure parameter distribution width increases with temperature and its maximum is observed for increasing b_2^0 values.

5.4. Discussion

For Fe^{3+}, the spectrum calculated at 120 K is in agreement with the experimental TMFG spectrum whatever the frequency band (S, X and Q). The corresponding fine structure parameter distribution is similar to the Czjzek distribution used to simulate the TMFG:Fe^{3+} spectrum; the maximum is observed for the same b_2^0 value: 0.1 cm^{-1}.

For Cr^{3+}, a satisfying agreement is not so clearly obtained. The spectrum calculated at 200 K is in agreement with the experimental X band spectrum. However, high b_2^0 values induce a calculated $g_{eff} = 5.0$ resonance at Q band higher than the experimental one. Conversely, at 120 K, the intensity of the calculated $g_{eff} = 1.97$ resonance is too high. But at this temperature, the fine structure parameter distribution has its maximum at the same value ($b_2^0 = 0.25$ cm^{-1}) as the Czjzek one used to simulate TMFG:Cr^{3+}. It may be inferred that the $P(b_2^0, \lambda)$ values at 120 K are slightly too large for small b_2^0 values. In other words, among the 576 octahedra, some of them should be more distorted.

Table 4. Distance and angle standard deviations.

Model	$\langle\lvert d_i - \langle d\rangle\rvert\rangle$	$\langle\lvert\alpha_i - 90°\rvert\rangle$	$\langle\lvert\beta_i - 180°\rvert\rangle$
GaF_3 (120 K)	0.021 Å	2.4°	4.3°
$CsZnGaF_6$	0.022 Å	2.1°	2.9°

Table 5. Root mean square deviation.

Model	$\sqrt{\sum_{i=1}^{n}(d_i - \langle d\rangle)^2/n}$	$\sqrt{\sum_{i=1}^{n}(\alpha_i - \langle\alpha\rangle)^2/n}$
GaF_3 (120 K)	2.65×10^{-2} Å	2.95°
$CsZnGaF_6$	2.76×10^{-2} Å	2.60°
FeF_3 [8]	5×10^{-2} Å	13°

Nevertheless, the acceptable agreement obtained at this temperature allows to assume that the 120 K MD calculation gives the best description of the local disorder in TMFG. Moreover, the distance and angle distributions are nearly the same as those deduced from the $CsZnGaF_6$ model (figure 10); the distance and perpendicular angle standard deviations $\langle\lvert d_i - \langle d\rangle\rvert\rangle$ and $\langle\lvert\alpha_i - 90°\rvert\rangle$ are very close (table 4). Only angles between

opposite bonds distribution have different trends (see 5.3); for these angles, the standard deviation calculation $\langle|\beta_i - 180°|\rangle$ gives quite different values (table 4). The $CsZnGaF_6$ model leads to a high probability of obtaining the angle between opposite bonds close to 180°. Moreover, M–F distance values are randomly attributed without worrying about system stability. Therefore, we put more trust in the MD model calculation. In table 5, root mean square deviation values are reported for our models and the random network of corner-sharing octahedra representing the structure of amorphous FeF_3 [8]. The 'FeF_3 model' leads to higher values especially for angles difficult to take into account in our EPR spectra reconstruction.

6. Conclusion

The use of the Czjzek distribution for Cr^{3+} and Fe^{3+} spectra reconstruction in TMFG have been validated since the fine structure parameter distributions generated by our models are similar to the Czjzek one.

The two models give a quantification of the local disorder within TMFG, $CsZnGaF_6$ and amorphous GaF_3 constituent octahedra. Octahedra are shown to be but slightly distorted; the Ga–F distances are nearly all in the interval $d_0 \pm 0.04$ Å and the angular deviations from regular octahedra are generally less than 5°. Our results are in agreement with EXAFS study leading to a narrow distance distribution [20]. Compared to EXAFS, the advantage of this study is to quantify the angular distortions.

Our results are quite different from those obtained through previous MD calculations [24] and 'quasicrystalline' simulations of diffraction data [31] which lead to strongly distorted octahedra. It may be outlined that these models have given satisfactory descriptions of the medium-range ordering but were not tested on experimental measurements sensitive to short-range order.

Finally, our results show unambiguously that the short-range order in TMFG has strong similarities with crystalline structures built up from MF_6 octahedra. $CsZnGaF_6$ gives satisfying results and has a particular interest, due to its chemical composition (CsF, ZnF_2, GaF_3) close to the PZG glass one (PbF_2, ZnF_2, GaF_3); the PZG glass and $CsZnGaF_6$ network are built with the same kind of octahedron.

Acknowledgments

The authors are indebted to J M Grenèche for recording the Mössbauer spectrum shown in this work and for many fruitful discussions. They also acknowledge P Simon for recording the Q band spectra.

References

[1] Le Bail A, Jacoboni C and de Pape R 1985 *Mater. Sci. Forum* **6** 441
[2] Boulard B, Jacoboni C and Rousseau M 1989 *J. Solid State Chem.* **80** 17
[3] Lopez-Herrera M E, Grenèche J M and Varret F 1983 *Phys. Rev.* B **28** 4944
[4] Grenèche J M, Varret F, Leblanc M and Ferey G 1987 *Solid State Commun.* **63** 435
[5] Leblanc M, Ferey G, Grenèche J M, Le Bail A, Varret F, de Pape R and Pannetier J 1985 *J. Physique Coll.* **12** C8 175
[6] Grenèche J M, Leblanc M, Varret F and Ferey G 1986 *Hyperfine Interact.* **27** 317
[7] Grenèche J M, Le Bail A, Leblanc M, Mosset A, Varret F, Galy J and Ferey G 1988 *J. Phys. C: Solid State Phys.* **21** 1351
[8] Grenèche J M, Teillet J and Coey J M D 1987 *J. Physique* **48** 1709

[9] Legein C, Buzaré J Y, Emery J and Jacoboni C 1995 *J. Phys.: Condens. Matter* **7** 3853
[10] Czjzek G, Fink J, Götz F, Schmidt H, Coey J M D, Rebouillat J P and Liénard A 1981 *Phys. Rev.* B **23** 2513
[11] Newman D J 1971 *Adv. Phys.* **20** 197
[12] Le Bail A, Jacoboni C and de Pape R 1986 *J. Solid State Chem.* **61** 188 .
[13] Jacoboni C, Le Bail A and de Pape R 1983 *Glass Technol.* **24** 164
[14] Auriault N, Guéry J, Mercier A M, Jacoboni C and de Pape R 1985 *Mater. Res. Bull.* **20** 309
[15] Boulard B and Jacoboni C 1990 *Mater. Res. Bull.* **25** 671
[16] Houlbert S 1992 *Thesis* University of Caen
[17] Legein C, Buzaré J Y and Jacoboni C 1995 *J. Solid State Chem.* submitted
[18] Shannon R D 1976 *Acta Crystallogr.* A **32** 751
[19] Legein C, Buzaré J Y and Jacoboni C 1995 *J. Non-Cryst. Solids* at press
[20] Calage Y and Varret F 1978 *Chem. Phys. Lett.* **55** 380
[21] Varret F and Courbion G 1980 *Revue Phys. Appl.* **15** 1149
[22] Czjzek G 1982 *Phys. Rev.* B **25** 4908
[23] Grenèche J M, Varret F and Teillet J 1988 *J. Physique* **49** 243
[24] Boulard B, Le Bail A, Jacoboni C and Simmons J H 1988 *Mater. Sci. Forum* **32–33** 61
[25] Le Bail A, Jacoboni C and de Pape R 1984 *J. Solid State Chem.* **52** 32
[26] Simmons J H, Faith R, and O'Rear G 1987 *Mater. Sci. Forum* **19–20** 121
[27] Fumi F G and Tosi M P 1964 *J. Phys. Chem. Solids* **25** 31, 45
[28] Busing W R 1972 *J. Chem. Phys.* **57** 3008
[29] Brewer F M, Carton G and Goodgame D M L 1959 *J. Inorg. Nucl. Chem.* **9** 56
[30] Verlet L 1967 *Phys. Rev.* **159** 98
[31] Le Bail A, Jacoboni C and de Pape R 1985 *J. Physique Coll.* **12** C8 163